

Microscopic model of Purcell enhancement in hyperbolic metamaterials

Alexander N. Poddubny,^{1,2} Pavel A. Belov,^{1,3} Pavel Ginzburg,⁴ Anatoly V. Zayats,⁴ and Yuri S. Kivshar^{1,5}

¹*National Research University for Information Technology,
Mechanics and Optics (ITMO), St. Petersburg 197101, Russia*

²*Ioffe Physical-Technical Institute of the Russian Academy of Science, St. Petersburg 194021, Russia*

³*School of Electronic Engineering and Computer Science,
Queen Mary University of London, London E1 4NS, UK*

⁴*Department of Physics, Kings College London, London WC2R 2LS, UK*

⁵*Nonlinear Physics Center and Center for Ultrahigh-bandwidth Devices for Optical Systems (CUDOS),
Research School of Physics and Engineering, Australian National University, Canberra ACT 0200, Australia*

We study theoretically a dramatic enhancement of spontaneous emission in metamaterials with the hyperbolic dispersion modeled as a cubic lattice of anisotropic resonant dipoles. We analyze the dependence of the Purcell factor on the source position in the lattice unit cell and demonstrate that the optimal emitter position to achieve large Purcell factors and Lamb shifts are in the local field maxima. We show that the calculated Green function has a characteristic cross-like shape, spatially modulated due to structure discreteness. Our basic microscopic theory provides fundamental insights into the rapidly developing field of hyperbolic metamaterials.

PACS numbers: 42.50.-p, 74.25.Gz, 78.70.-g

I. INTRODUCTION

Engineering light-matter interaction in nanostructured environment has recently been the focus of active studies [1–7]. In particular, the so-called hyperbolic metamaterials described by an uniaxial medium where the main components of dielectric and magnetic tensor have different signs, have attracted significant attention [8–10]. Realizations of the regime of the hyperbolic medium with negative components of the dielectric tensor have been reported for magnetized plasma [11], graphite [12], for metamaterials based on nanorod assemblies [13–15] and for layered metal-dielectric structures [2, 16, 17]. In this regime, light wavevectors at a given frequency fill a surface of a hyperbolic shape, so that the area of hyperbolic isofrequency surface, giving the photonic density of states, is infinite. As the result, the spontaneous emission rate becomes infinite in the case of ideal hyperbolic medium [2, 18].

Experimental reports on the Purcell factor enhancement, describing the spontaneous emission rate modification, in hyperbolic metamaterials are already available [2, 19–21]. Theoretical studies for various models have been also performed [22]. It has been shown that the Purcell factor should not actually diverge. It is rather determined by a cutoff in the wavevector space, stemming from spatial inhomogeneity of the medium [23–25], a finite distance from the source to the medium [26, 27], nonlocality of dielectric response [28], or finite size of the emitter [29].

The basic solid state model of either natural or artificial material is a periodic lattice of unit cells. We adopt this model and consider hyperbolic material as the infinite cubic crystal of interacting resonant point dipoles. Similar models have been developed for various systems including lattices of quantum dots [30], optical atomic lattices [31, 32], γ -ray resonant nuclear scattering [33]

as well as the discrete-dipole-approximation of the light scattering theory [34]. This general approach, despite certain approximations, has been successfully applied to the lattices of split-ring resonators [35, 36].

In this paper, we study optical properties of the infinite cubic crystal of resonant interacting point dipoles polarizable only in one direction (see Fig. 1). This model allows us to reproduce the hyperbolic isofrequency surfaces of the uniaxial anisotropic metamaterials and accounts for the discrete character of metamaterials. Within this microscopic model of hyperbolic metamaterial, we investigate the influence of emitter position within the unit cell of the metamaterial on its radiation properties.

The paper is organized as follows. Section II outlines our theoretical model and approach. Calculated dispersion and lattice Green function are discussed in Sec. III. Section IV is devoted to the numerical and analytical results for the Purcell factor and Lamb shift in metamaterials with hyperbolic dispersion.

II. DISCRETE DIPOLE MODEL

We consider an infinite periodic cubic lattice \mathbf{r}_j of the point dipoles, characterized by the period a , and embedded in vacuum. Our approach can be straightforwardly generalized to allow for background dielectric constant $\varepsilon \neq 1$. The emitter inside the lattice is modeled by a radiating dipole \mathbf{p}_0 is placed at the point \mathbf{r}_0 . Structure geometry is sketched on Fig. 1. The self-consistent electric field satisfies the following equation

$$\nabla \times \nabla \times \mathbf{E} - q^2 \mathbf{E} = 4\pi q^2 \mathbf{P}, \quad (1)$$

where $q = \omega/c$ is the wavevector at the frequency ω . The quantity \mathbf{P} in Eq. (1) is the net polarization of the lattice

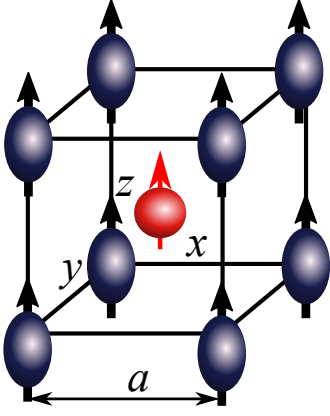


FIG. 1: (Color online) Schematic illustration of the unit cell of the cubic dipole lattice with embedded light source.

dipoles and the emitter:

$$\mathbf{P} = \mathbf{d}_0 \delta(\mathbf{r} - \mathbf{r}_0) + \sum_j \mathbf{p}_j \delta(\mathbf{r} - \mathbf{r}_j). \quad (2)$$

All the dipoles \mathbf{p}_j are characterized by the identical polarizability tensor $\hat{\alpha}$

$$\mathbf{p}_j = \hat{\alpha} \mathbf{E}_{\text{ext}}(\mathbf{r}_j), \quad (3)$$

Our goal is to determine the total electric field and polarizations, induced in the structure by the radiating dipole \mathbf{d}_0 . This procedure includes field expansion over the Bloch eigenmodes with wavevectors \mathbf{k} , for which Eqs. (1),(2) are independent. The results in a coordinate space are obtained by inverse Fourier transformation. In particular, the polarizations of lattice dipoles read

$$\mathbf{p}_j = \int_{(\text{BZ})} \frac{V_0 d^3 k}{(2\pi)^3} e^{i\mathbf{k}\mathbf{r}_j} \hat{\alpha} [\hat{1} - \hat{C}(\mathbf{k})\hat{\alpha}]^{-1} \hat{G}_{0,\mathbf{k}}(-\mathbf{r}_0) \mathbf{d}_0 \quad (4)$$

where $V_0 = a^3$ is the unit cell volume, the integration takes place over the Brillouin zone $|k_m| < \pi/a$, $m = x, y, z$, and $\hat{1}$ is 3×3 unity matrix. Radiating dipole position \mathbf{r}_0 enters Eq. (4) and thus determines the efficiency of the lattice excitation. The quantity \hat{C} in Eq. (4) is the tensor interaction constant of the lattice, defined as [35]

$$\hat{C}(\mathbf{k}) = \lim_{\mathbf{r} \rightarrow 0} [\hat{G}_{0,\mathbf{k}}(\mathbf{r}) - \hat{G}_0(\mathbf{r})] + \frac{2iq^3}{3} \hat{1}, \quad (5)$$

where $\hat{G}_{0,\mathbf{k}}$ is the Green function of the photon with Bloch vector \mathbf{k} ,

$$\hat{G}_{0,\mathbf{k}}(\mathbf{r}) = \sum_j \hat{G}_0(\mathbf{r} - \mathbf{r}_j) e^{i\mathbf{k}\mathbf{r}_j}. \quad (6)$$

and \hat{G}_0 is the free photon Green function

$$\hat{G}_0(\mathbf{r}) = [q^2 + \nabla \nabla] \hat{1} \frac{e^{iqr}}{r}. \quad (7)$$

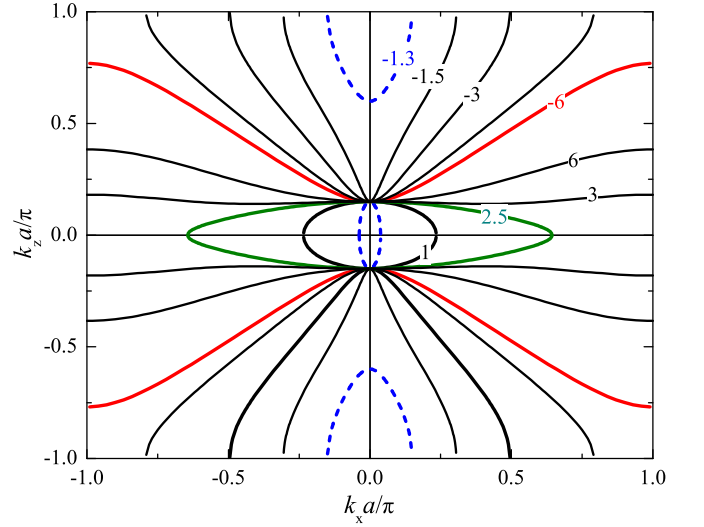


FIG. 2: (Color online) Isofrequency curves in xz plane, calculated for different dipole polarizabilities $\alpha_{0,zz}$. Normalized polarizability $4\pi\alpha_{0,zz}/a^3$ is indicated near each curve. Calculated was performed at $qa = 0.15\pi$.

The infinite lattice sums (6) may be found either by Ewald summation [37] or by a Floquet-type summation [35]. We have used the approach from Ref. 35, since it is preferential for fast evaluation of the integral (4). Electric field in the structure is given by the sum of the waves emitted by all the dipoles ,

$$\mathbf{E}(\mathbf{r}) = \hat{G}_0(\mathbf{r} - \mathbf{r}_0) \mathbf{p}_0 + \sum_j \hat{G}_0(\mathbf{r} - \mathbf{r}_j) \mathbf{p}_j. \quad (8)$$

Eq. (8), by definition provides the Green function for the source embedded in the dipole lattice. Second term in Eq. (8) is given by Eq. (4) where $e^{i\mathbf{k}\mathbf{r}_j}$ is replaced by $\hat{G}_{0,\mathbf{k}}(\mathbf{r})$.

From now we restrict ourselves to the case of uniaxial dipoles, when the only non-zero component of the tensor $\hat{\alpha}$ is α_{zz} . We assume that the radiating dipole \mathbf{d}_0 is also directed along z axis. The TM-polarized Bloch eigenmodes of the system with given wavevector \mathbf{k} are found[35, 36] from the poles of Eq. (4)

$$\frac{1}{\alpha_{zz}} - C(\mathbf{k}) = 0, \quad (9)$$

where $C(\mathbf{k}) \equiv C_{zz}(\mathbf{k})$. Note, that Eq. (9) is real for vanishing losses, because the imaginary part of the interaction constant (5) cancels out with the radiative decay term in the polarizability:

$$\frac{1}{\alpha_{zz}} = \frac{1}{\alpha_{0,zz}} - \frac{2iq^3}{3} \hat{1}. \quad (10)$$

Here $\alpha_{0,zz}$ is the so-called bare dipole polarizability, calculated neglecting radiative decay [38]. Effective medium approximation for the solutions of Eq. (9) are the extraordinary TM-polarized modes, with the dispersion given

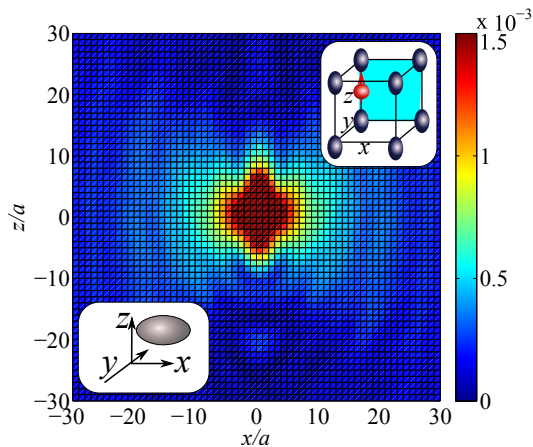


FIG. 3: (Color online) Spatial distribution of the dipole moments $|p_z(\mathbf{r})|/p_0$ in the elliptic regime with $\alpha_{0,zz} = a^3/(4\pi)$. Insets schematically illustrate the geometry and the isofrequency surfaces in wavevector space. Calculation was performed at $qa = 0.15\pi$ and $\mathbf{r}_0 = 0.5a\hat{z}$.

by [39]

$$q^2 = \frac{k_x^2 + k_y^2}{\varepsilon_{zz}} + k_z^2. \quad (11)$$

Here ε_{zz} is the Maxwell-Garnett effective dielectric constant of the hyperbolic medium

$$\varepsilon_{zz} = 1 + \frac{1}{V/(4\pi\alpha_{0,zz}) - 1/3}, \quad (12)$$

in the same approximation $\varepsilon_{xx} = \varepsilon_{yy} = 1$.

III. DISPERSION AND GREEN FUNCTION

In this Section we first discuss the dispersion of the Bloch waves in the dipole lattice (Sec. III A) and then investigate in detail the emission pattern of the dipole embedded in the lattice (Sec. III B).

A. Isofrequency curves

Isofrequency curves in the (k_z, k_x) plane, found from Eq. (9) for different polarizabilities $\alpha_{0,zz}$, are shown on Fig. 2. Depending on the polarizability, dispersion curves are either elliptic or hyperbolic, in agreement with Eq. (12). The curves are generally well described by the effective medium approximation (11). However, an intermediate “mixed” regime is possible for $\alpha_{0,zz} \approx -1.3a^3/(4\pi)$ (blue dashed curve), when two Bloch modes with hyperbolic and elliptic dispersion coexist in the structure. Such isofrequency curves can not be described by the Maxwell-Garnett theory Eqs. (11),(12), which predicts only one TM mode for given frequency. They were analyzed in Ref. 35 in more details and can be obtained

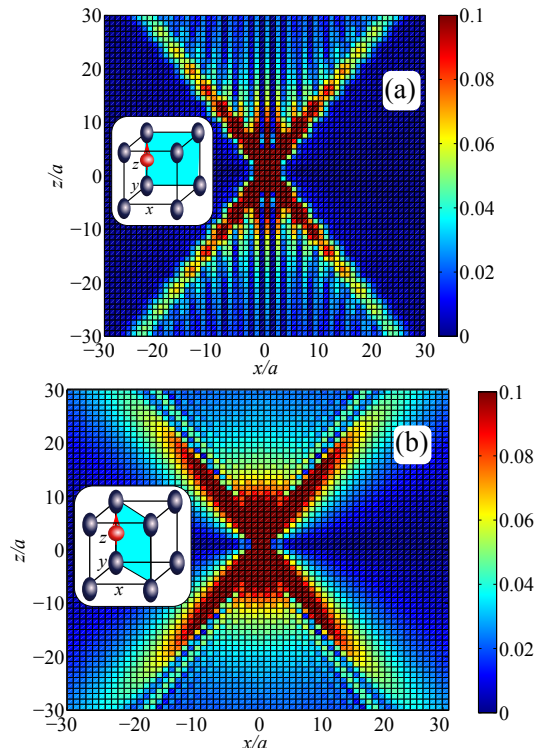


FIG. 4: (Color online) Spatial distribution of the dipole moments $|p_z(\mathbf{r})|/p_0$ in the hyperbolic regime, excited by the point emitter. Panels (a) and (b) show the distribution in the planes $y = 0$ and $x = y$, respectively. Insets schematically illustrate the geometry and the isofrequency surfaces in wavevector space. Calculation was performed at $\alpha_{0,zz} = -6a^3/(4\pi)$ and the same other parameters as Fig. 3.

in the effective medium model when nonlocal effects are taken into account [40, 41].

B. Green function

Here we will focus on the spatial distribution (4) of the dipole moments $|p(\mathbf{r}_j)|$ in the discrete lattice under the point dipole excitation. Results of calculation for the dipole polarizabilities $\alpha_{0,zz} = a^3/(4\pi)$ and $\alpha_{0,zz} = -6a^3/(4\pi)$, corresponding to elliptic and hyperbolic regimes, are shown on Fig. 3 and Fig. 4, respectively. Calculation demonstrates that the distribution is qualitatively different in hyperbolic regime: the pattern is strongly anisotropic and has characteristic cross-like shape, see Fig. 4. Moreover, in hyperbolic case the pattern depends on the azimuthal direction: it has distinct vertical ripples in the plane $y = 0$ (Fig. 3a), which are absent in the plane $y = x$ (Fig. 3b).

To understand these results it is instructive to compare them with Green function in the effective medium approximation, see Fig. 5. This approximation allows one to obtain the solution in a closed form [8, 42]. In the case of a vertical orientation of the radiating dipole,

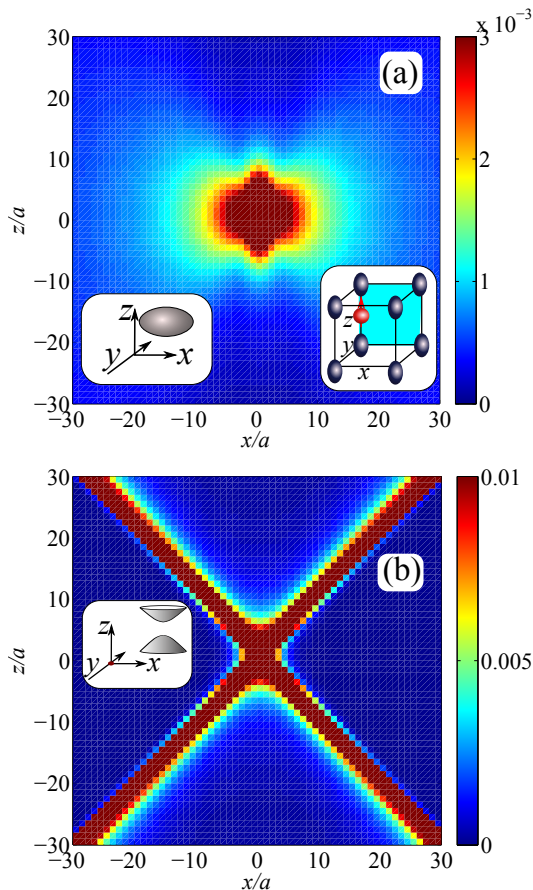


FIG. 5: (Color online) Spatial distribution of the polarization $P_{\text{eff},z}(\mathbf{r})/(p_0 a^3)$ induce by the point source in (a) effective elliptic medium with $\varepsilon_{zz} = 2.5$ and (b) effective hyperbolic medium with $\varepsilon_{zz} = -1$. Insets schematically illustrate the geometry and the isofrequency surfaces in wavevector space. Polarization is evaluated at the discrete lattice sites \mathbf{r}_j in the xz plane. Other calculation parameters are the same as for Fig. 3.

$\mathbf{p}_0 \parallel z$, Green function reads

$$\mathbf{E}_{\text{eff}}(\mathbf{r}) = (q^2 + \nabla\nabla)p_0 \hat{\mathbf{z}} \frac{e^{iqR}}{R},$$

$$R = \sqrt{\varepsilon_{zz}(x-x_0)^2 + \varepsilon_{zz}(y-y_0)^2 + (z-z_0)^2}. \quad (13)$$

This is generalization of Eq. (7) in the case of uniaxial medium. The relation between electric field and polarization in the effective medium model is local,

$$4\pi \mathbf{P}_{\text{eff}} = (\varepsilon_{\text{eff}} - 1) \mathbf{E}_{\text{eff}}. \quad (14)$$

It should be stressed that the effective medium approximation is not applicable on the spatial scales smaller than the lattice constant a . Consequently, the problem of point radiating dipole in discrete structure can not be reduced to the effective medium one. The effects of the radiating dipole position within the unit cell are also beyond the effective medium approximation. Thus, the

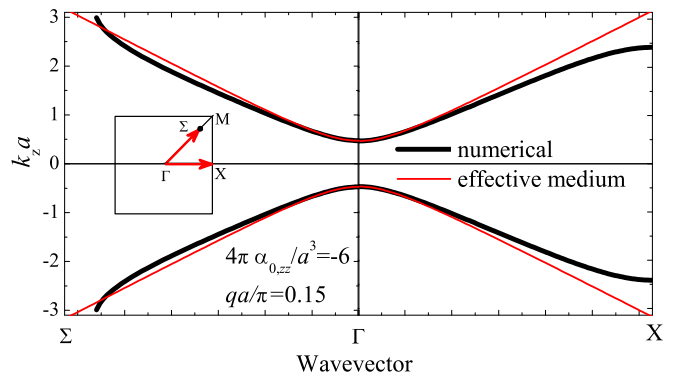


FIG. 6: Isofrequency curves of the dipole lattice in the hyperbolic regime. Solid and thin lines correspond to numerical calculation and effective medium approximation Eq. (11). Other parameters are the same as for Fig. 4. The inset schematically indicates the Brillouin zone of the square lattice, point Σ corresponds to $k_x = k_y = \pi/(\sqrt{2}a)$.

results of two models, discrete and effective, may be compared only qualitatively.

In order to clarify the ambiguity we have evaluated on Fig. 5 the polarization (14) at the discrete set of square lattice points \mathbf{r}_j and the radiating dipole is located at the point $\mathbf{r}_0 = 0.5a\hat{\mathbf{z}}$, see the inset of panel (a). Fig. 5a and Fig. 5b show the spatial distribution of the polarization Eq. (14) for the values effective dielectric constants off $\varepsilon_{zz} = 2.5$ and $\varepsilon_{zz} = -1$, corresponding to Fig. 3 and Fig. 4. In the case of the material with elliptic dispersion the emission pattern is qualitatively the same as for the isotropic medium. The near field is concentrated at the emitter origin, $\mathbf{r} = \mathbf{r}_0$, while the far-field is emitted perpendicularly to the dipole axis. The pattern changes dramatically in the hyperbolic case (Fig. 5b). The distribution has a distinct cross-like shape, typical for hyperbolic medium [8, 11]. In the elliptic case, the only field singularity is that at the origin $R = |\mathbf{r} - \mathbf{r}_0| = 0$. In the hyperbolic medium this singular point becomes a conical surface, where the field intensity is concentrated. Radiated waves are propagating within the cone $R^2 > 0$, and are evanescent outside this cone. Energy flow directions are normal to the isofrequency surfaces, so such cone in \mathbf{r} -space is a direct counterpart of the hyperbolic dispersion curves in \mathbf{k} -space.

Comparing numerical and effective medium results, Fig. 3 and Fig. 3a, we see that in the elliptic case the Green function is qualitatively the same as in the effective medium approximation. Weak spatial modulation of the dipole moments $|p(\mathbf{r}_j)|$, seen on Fig. 3, is related to the deviations from the effective medium theory Eq. (13), which, as mentioned above, is not completely valid for the point excitation. Distinct cross-like distribution of Fig. 4a is a fingerprint of the hyperbolic regime, similar to the effective medium approximation of Fig. 5b. Comparing Fig. 5b and Fig. 4a, we see, that in the discrete case the singularity in the effective medium solution (13) at the conical surface $R = 0$ is smeared out and even

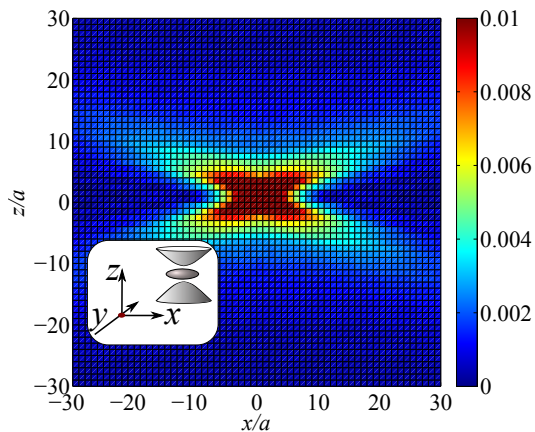


FIG. 7: (Color online) Spatial distribution of the dipole moments $|p_z(\mathbf{r})|/p_0$ in the mixed hyperbolic-elliptic regime with $\alpha_{0,zz} = -1.3a^3/(4\pi)$. Insets schematically illustrate the geometry and the isofrequency surfaces in wavevector space. Other calculation parameters are the same as for Fig. 5.

vanishes at large enough distances, where the effective approximation also breaks down. This is qualitatively explained by the presence of the wavevector cutoff $\sim \pi/a$. The second striking difference between Fig. 4 and its effective medium counterpart Fig. 5b is the strong spatial modulation of the distribution in the $y = 0$ plane, manifested as vertical ripples. Such modulation is obviously beyond the effective medium approximation of Fig. 5b. In particular, the ripples on Fig. 4(a) turn out to be the result of the interference of the Bloch waves with wavevectors $k_x = \pm\pi/a$, corresponding to the boundaries of the Brillouin zone. To check this hypothesis we have plotted on Fig. 6 the isofrequency curves in Γ -X and Γ -M directions. Interference pattern in the planes $y = 0$ and $y = x$ should depend on the dispersion along Γ -X and Γ -M, respectively. Since $dk_z/dk_x = 0$ at $k_x = \pi/a$ (right panel of Fig. 6), there is a singularity in the density of states propagating along x direction, promoting the vertical ripples. This singularity is absent for the Γ -M direction, where the behavior of the isofrequency curves at the Brillouin zone edge is different. Panels (a) and (b) of Fig. 4 present the spatial distribution (4) of the dipole moments $|p(\mathbf{r}_j)|$ in the planes $y = 0$ and $y = x$, respectively. We see that the spatial modulation in the plane $y = x$ is absent, cf. Fig. 4a and Fig. 4b, which corroborates our explanation. The discovered effect can be thought of as the manifestation of the Van Hove band edge singularity [43] in the Green function [44].

Discrete Green function calculated for the dipole polarizability $\alpha_{0,zz} = -1.3a^3/(4\pi)$, corresponding to mixed elliptic-hyperbolic regime, is shown on Fig. 7. In this case the ripples are absent, because the isofrequency curves do not reach the Brillouin zone boundary $k_x = \pm\pi/a$, see dashed curve on Fig. 2. Far-field emission along x direction is possible due to the modes with elliptic dispersion, providing weak background to the field of the hyperbolic modes.

IV. PURCELL FACTOR

Here we investigate the role of the discreteness on the Purcell factor determining the characteristics of the spontaneous emission of the radiating dipole inside the material. The Purcell factor f and the Lamb shift l for the radiating dipole can be found from the Green function (8), evaluated at the dipole origin [4, 5, 45], see also Ref. 46:

$$f + il = 1 + \frac{3iE_z(\mathbf{r}_0)}{2q^3p_0}. \quad (15)$$

Here the dimensionless Lamb shift l is formally understood as a radiative correction to the resonance frequency of the radiating two-level system, normalized to its free space decay rate. Gathering Eqs. (15),(8),(4) together, we find the result in a compact form

$$f + il = \frac{3i}{2q^3} \int_{(BZ)} \frac{V_0 d^3k}{(2\pi)^3} \frac{|G_{\mathbf{k},zz}(\mathbf{r}_0)|^2}{1/\alpha_{zz} - C(\mathbf{k}) - i0}. \quad (16)$$

The frequency ω , entering the wavevector q in Eq. (16), is determined by the transition energy of the radiating dipole \mathbf{d}_0 . It is clear from the structure of Eq. (16), that the Purcell factor is determined by the pole contribution, corresponding to emission of photons with the dispersion given by Eq. (9). We note, that the first term in right-hand-side of Eq. (15) has canceled out in Eq. (16) with the pole contribution in the free space Green function $G_{\mathbf{k},zz}(\mathbf{r}_0)$ at $q = k$. We stress, that despite the classical formulation of the problem, the results for the emission rate and photon Green function may be equivalently obtained by the quantum-mechanical calculation, either using the Fermi Golden rule [5] or the local quantization framework [4].

Numerical results for the dependence of the Purcell factor on the radiating dipole position within the unit cell of the structure are presented in Figs. 8, Fig. 9. Fig. 10 shows the frequency dependence of the Purcell factor. Figures demonstrate that the Purcell factor is much larger in hyperbolic regime than in the elliptic one. It is very sensitive to the dipole position and strongly increases when the dipole approaches the lattice nodes. Before discussing these results in more details it is instructive to compared them with the analytical theory.

A. Analytical results

Here we focus on the Purcell factor in the quasi-static limit $q \ll \pi/a$. Eq. (16) can be then reduced to

$$f = \frac{3}{2q^3} \frac{V_0 |G_{zz,stat}(\mathbf{r}_0)|^2}{(2\pi)^2} \int dk_x dk_y \left| \frac{dC(\mathbf{k})}{dk_z} \right|_{k_z(k_x, k_y)}^{-1}, \quad (17)$$

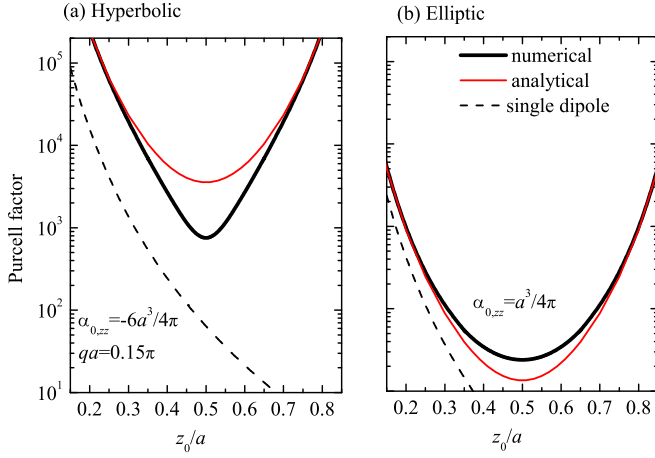


FIG. 8: (Color online) Purcell factor in the (a) hyperbolic and (b) elliptic regime as function of the source coordinate z_0 for $x_0 = y_0 = 0$. Thick solid black, thin solid red, and dashed black curves correspond to numerical calculations, the analytical results of Eq. (20) (panel a), Eq. (23) (panel b), and to a single dipole with corresponding polarizability (Eq. (25)), respectively. Dashed curves are results (17) for source near single dipole at $\mathbf{r} = 0$. Other parameters as the same as for Fig. 4.

where the interaction constant in the effective medium approximation reads [36]

$$C(\mathbf{k}) = \frac{4\pi q^2 - k_z^2}{V_0 k^2 - q^2} + \frac{4\pi}{3V_0} + \frac{2iq^3}{3}. \quad (18)$$

The integral over k_z in (16) is determined by the residues at the wavevectors $\pm k_z(k_x, k_y)$, being the solutions of Eq. (9) at given frequency. Integration over k_x and k_y in Eq. (17) is restricted to those vectors within the two-dimensional Brillouin zone, for which such solution exists. The quantity $G_{zz,\text{stat}}(\mathbf{r}_0)$ in (17) is the quasistatic approximation of the Green function (6): $G_{zz,\text{stat}}(\mathbf{r}_0) \equiv G_{\mathbf{k},zz}(\mathbf{r}_0)|_{\mathbf{k}=0,q=0}$. The value of $G_{zz,\text{stat}}$ is determined by

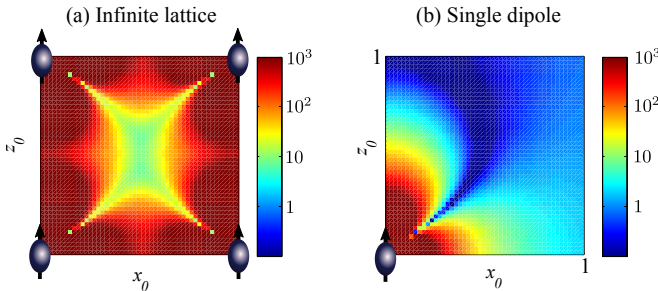


FIG. 9: (Color online) (a) Purcell factor in hyperbolic medium as function of the source position in the unit cell. (b) Calculation in single-dipole approximation Eq. (25). Calculation was carried out at $y_0 = 0$ and the same other parameters as for Fig. 4. Radiating dipole coordinates change within the square $0 \leq x_0 \leq 1$, $0 \leq z_0 \leq 1$. Colors correspond to logarithmic scale, identical for both panels.

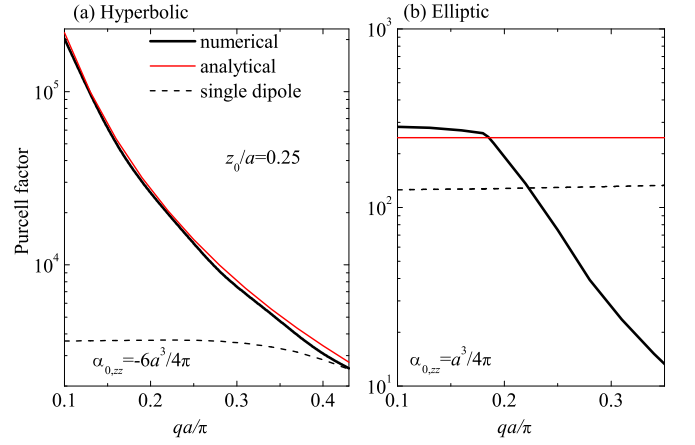


FIG. 10: (Color online) Purcell factor in (a) hyperbolic and (b) elliptic regime as function of the frequency qa for $\mathbf{r}_0 = 0.25a\hat{\mathbf{z}}$. Notation and other parameters as the same as for Fig. 8.

the near field of the lattice dipoles, closest to the radiating one. Maximum Purcell factor can be then expected when the source is located on the vertical edge of the elementary cell, i.e. $x_0 = y_0 = 0, z_0 \neq 0$. In this case $G_{zz,\text{stat}}(z_0)$ can be reduced to

$$G_{zz,\text{stat}}(z_0) \approx \frac{2}{z_0^3} + \frac{2}{(a - z_0)^3} \quad (19)$$

and grows dramatically when the emitter approaches the lattice node. Evaluating the derivative in Eq. (17) by means of Eq. (18) and performing the integration, we obtain the analytical result for the Purcell factor

$$f_{\text{hyp}} = \frac{(\varepsilon - 1)^2}{32\pi^2} \left(\frac{k_{z,\text{max}}}{q} \right)^3 |V_0 G_{zz,\text{stat}}(z)|^2 \quad (20)$$

in the hyperbolic medium. Here $k_{z,\text{max}} \gg q$ is the cutoff for the wavevector k_z , existing due to the finite extent of the Brillouin zone. Its value depends on the effective dielectric constant,

$$k_{z,\text{max}} \approx \begin{cases} \frac{\pi}{a}, & -1 \leq \varepsilon \leq 0 \\ \frac{\pi}{a\sqrt{|\varepsilon_{zz}|}}, & \varepsilon_{zz} \leq -1. \end{cases} \quad (21)$$

Thus, Eq. (20) provides a compact analytical result for the Purcell factor in the lossless hyperbolic medium. Its general structure can be understood as follows: the factor $(k_{z,\text{max}}/q)^3 \sim 1/(qa)^3$ describes the enhancement of the photonic density of states as compared to the vacuum. The second factor $|V_0 G_{zz,\text{stat}}(z)|^2$ reflects the coordinate dependence of the Purcell factor, governed by the near-field of the neighboring dipoles. Near the lattice nodes Eq. (20) can be simplified to

$$f_{\text{hyp}}(q, z \rightarrow 0) \approx \frac{\pi(\varepsilon - 1)^2 a^3}{8q^3 |z|^6}, \quad (22)$$

where we assumed that $|\varepsilon| \leq 1$.

Similar calculation can be also performed in the elliptic case, when $\varepsilon_{zz} > 0$. It should be noted, that in the effective medium approximation, the Purcell factor for the axial dipole in the elliptic medium is unity, independently of the value of ε_{zz} [29]. Local-field corrections can still promote high decay rate. The answer reads

$$f_{\text{ell}} = |G_{\text{stat},zz}|^2 \left| \frac{V_0(\varepsilon - 1)}{4\pi} \right|^2. \quad (23)$$

This expression depends on the local field intensity, similarly Eq. (20), but is smaller by the factor

$$\frac{f_{\text{hyp}}}{f_{\text{ell}}} = \frac{k_{z,\text{max}}^3}{2q^3}, \quad (24)$$

since the density of states in elliptic medium is smaller. In order to distinguish between the local field effects and the collective effects due to density of states enhancement in the medium it instructive to analyze also the Purcell factor for a source located in vacuum near *single* dipole in the point $\mathbf{r} = 0$. The result reads [47]

$$f_1 = 1 + \frac{3}{2q^3} \text{Im}[\alpha_{zz} G_{0,zz}^2(\mathbf{r}_0)], \quad (25)$$

here the second term is the field of the emitter, reflected from the dipole. In the quasistatic limit $q \rightarrow 0$ Eq. (25) reduces to

$$f_1 = \left(1 + \frac{\alpha_{0,zz}}{|z^3|} \right)^2. \quad (26)$$

Both Eqs. (22) and (26) demonstrate divergency when z tends to zero. However, their dependence on the wavevector q is quite different: Eq. (22) diverges as $1/q^3$ at small q , while Eq. (26) does not depend on q at all. This divergency is a characteristic effect of photonic density of states enhancement in the hyperbolic medium [18, 24, 29].

B. Numerical results

Now we discuss the calculated dependence of the Purcell factor on the source position and on the transition frequency $\omega = cq$, shown on Fig. 8, Fig. 9 and Fig. 10. The calculation confirms the singular behavior of the Purcell factor in the hyperbolic case when the source approaches the lattice nodes (solid curve on Fig. 8a). The singularity is excellently described by analytical Eq. (20) (thin red curve). The interaction of the emitter with a single dipole (Eq. (25)) provides substantially smaller enhancements (dashed black curve), although it also diverges at $z = 0$ and $z = a$. Additional comparison of the exact calculation in medium with the result for a single dipole is presented by the Purcell factor dependence on the two coordinates x and z in the unit cell, shown

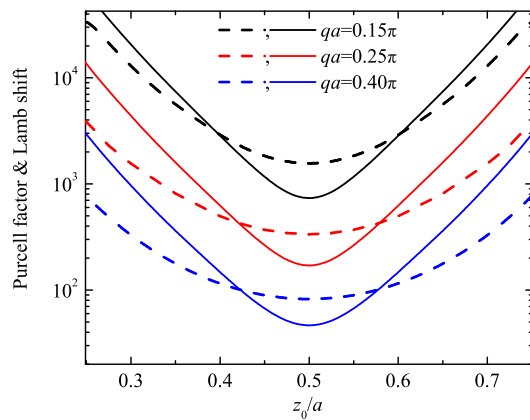


FIG. 11: (Color online) Purcell factor (solid lines) and Lamb shift (dashed lines) dependence on the coordinate z_0 of the source in the unit cell for different values of qa . Calculation parameters as the same as for Fig. 4.

on Fig. 9. Eq. (25), taking into account only single lattice dipole at the point $\mathbf{r} = 0$, satisfactorily reproduces the Purcell factor pattern near this point. Corresponding two-dimensional plot of the Purcell factor in the quadrant $0 \leq x, y \leq 1$ is shown in Fig. 9(b). Comparing two panels of Fig. 9 we see, that near the corner $\mathbf{r} = 0$ the angular dependence is approximately given by $(3 \cos^2 \theta - 1)^2$, where θ is a polar angle. Still, single dipole model with corresponding polarizability $\alpha_{0,zz} = -6a^3/(4\pi)$ considerably underestimates the absolute values of the Purcell factor. The saturation is different in the elliptic case, where all three approaches, namely numerical calculation according to Eq. (16), single dipole model (25) with $\alpha_{0,zz} = a^3/(4\pi)$ and analytical model (23) provide similar results, see Fig. 8b.

The failure of the single dipole model in the hyperbolic medium is also revealed in the frequency dependence of the Purcell factor, Fig. 10a. The dashed curve, calculated for single dipole, tends to the limit (26), which is frequency independent. However, the Purcell factor in the hyperbolic medium diverges at low frequencies as $1/q^3$, according to Eq. (22). The Lamb shift l , calculated in hyperbolic medium for different values of qa is presented in Fig. 11 by the dashed curves. Lamb shift is of the same order as the Purcell factor (dashed curve) and has similar near-field singularities at the node sites.

To summarize, Figs. 8–11 underline the importance of the local-field effects in the hyperbolic medium and confirm the collective origin of the spontaneous emission enhancement.

V. CONCLUSIONS

We have developed the analytical theory of light-matter coupling in discrete hyperbolic metamaterials in the framework of the discrete model of a cubic lattice

of uniaxial resonant dipoles. We have calculated Purcell factor, Lamb shift, and Green function for such a discrete model, and we have demonstrated that the optimal emitter position is in the local field maxima, close to the lattice nodes. We have demonstrated that the density of states is drastically enhanced in the hyperbolic regime as compared to other cases including vacuum, elliptic regime, or single resonant dipole case. As a result, a huge number of lattice dipoles are efficiently excited by the emitter, which has been visualized by calculating the Green function of the lattice. The Green function has a shape of a cone: the field propagates along the directions close to symmetry axis z and decays in the xy plane. Discrete character of the problem results in the strong spatial modulation of the Green function.

The calculated absolute values of the Purcell factor are rather challenging for the current realization of metamaterials. This is mainly due to the point dipole approximation we have utilized: as distance to the scatterers becomes comparable to their sizes, higher order multi-

poles must be accounted for. This will inevitably reduce the local field and suppress the Purcell factor. Achieving large density of states enhancement described by Eq. (24) is also not easy. Finally, the losses are inevitable and can significantly influence the numerical answers. Nevertheless, we believe that our results will remain qualitatively correct for more complex settings, and they provide an important insight into the physics of hyperbolic metamaterials.

Acknowledgments

This work has been supported by the Ministry of Education and Science of Russian Federation, the ‘‘Dynasty’’ Foundation, Russian Foundation for Basic Research, European project POLAPHEN, EPSRC (UK), and the Australian Research Council. The authors acknowledge useful discussions with C.R. Simovski.

-
- [1] Z. Jacob and V. M. Shalaev, *Science* **334**, 463 (2011).
 - [2] H. N. S. Krishnamoorthy, Z. Jacob, E. Narimanov, I. Kretzschmar, and V. M. Menon, *Science* **336**, 205 (2012).
 - [3] H. Gibbs, G. Khitrova, and S. Koch, *Nature Photonics* **5**, 273 (2011).
 - [4] W. Vogel and D.-G. Welsch, *Quantum Optics* (Wiley, Weinheim, 2006).
 - [5] E. L. Ivchenko, *Optical spectroscopy of semiconductor nanostructures* (Alpha Science International, Harrow, UK, 2005).
 - [6] A. Kavokin, J. Baumberg, G. Malpuech, and F. Laussy, *Microcavities* (Clarendon Press, Oxford, 2006).
 - [7] M. G. Silveirinha and S. I. Maslovski, *Phys. Rev. B* **85**, 155125 (2012).
 - [8] L. Felsen and N. Marcuvitz, *Radiation and scattering of waves* (Wiley Interscience, New York, 2003).
 - [9] I. V. Lindell, S. A. Tretyakov, K. I. Nikoskinen, and S. Ilvonen, *Microwave and Optical Technology Lett.* **31**, 129 (2001).
 - [10] D. R. Smith and D. Schurig, *Phys. Rev. Lett.* **90**, 077405 (2003).
 - [11] R. K. Fisher and R. W. Gould, *Phys. Rev. Lett.* **22**, 1093 (1969).
 - [12] J. Sun, J. Zhou, B. Li, and F. Kang, *Appl. Phys. Lett.* **98**, 101901 (2011).
 - [13] G. A. Wurtz, W. Dickson, D. O’Connor, R. Atkinson, W. Hendren, P. Evans, R. Pollard, and A. V. Zayats, *Opt. Express* **16**, 7460 (2008).
 - [14] M. A. Noginov, Y. A. Barnakov, G. Zhu, T. Tumkur, H. Li, and E. E. Narimanov, *Appl. Phys. Lett.* **94**, 151105 (2009).
 - [15] C. R. Simovski, P. A. Belov, A. V. Atrashchenko, and Y. S. Kivshar, *Adv. Materials* (2012), in press.
 - [16] J. Elser, V. A. Podolskiy, I. Salakhutdinov, and I. Avrutsky, *Appl. Phys. Lett.* **90**, 191109 (pages 3) (2007).
 - [17] A. A. Orlov, P. M. Voroshilov, P. A. Belov, and Y. S. Kivshar, *Phys. Rev. B* **84**, 045424 (2011).
 - [18] Z. Jacob, J. Kim, G. V. Naik, A. Boltasseva, E. E. Narimanov, and V. M. Shalaev, *Appl. Phys. B: Lasers and Optics* **100**, 215 (2010).
 - [19] M. A. Noginov, H. Li, Y. A. Barnakov, D. Dryden, G. Nataraj, G. Zhu, C. E. Bonner, M. Mayy, Z. Jacob, and E. E. Narimanov, *Opt. Lett.* **35**, 1863 (2010).
 - [20] X. Ni, S. Ishii, M. D. Thoreson, V. M. Shalaev, S. Han, S. Lee, and A. V. Kildishev, *Opt. Express* **19**, 25242 (2011).
 - [21] J. Kim, V. P. Drachev, Z. Jacob, G. V. Naik, A. Boltasseva, E. E. Narimanov, and V. M. Shalaev, *Opt. Express* **20**, 8100 (2012).
 - [22] C. L. Cortes, W. Newman, S. Molesky, and Z. Jacob, *ArXiv e-prints* (2012), 1204.5529.
 - [23] Z. Jacob, I. Smolyaninov, and E. Narimanov, *ArXiv e-prints* (2009), 0910.3981.
 - [24] S. I. Maslovski and M. G. Silveirinha, *Phys. Rev. A* **83**, 022508 (2011).
 - [25] I. Iorsh, A. Poddubny, A. Orlov, P. Belov, and Y. S. Kivshar, *Phys. Lett. A* **376**, 185 (2012).
 - [26] H. Xie, P. Leung, and D. Tsai, *Solid State Comm.* **149**, 625 (2009).
 - [27] O. Kidwai, S. V. Zhukovsky, and J. E. Sipe, *Opt. Lett.* **36**, 2530 (2011).
 - [28] W. Yan, M. Wubs, and N. Asger Mortensen, *ArXiv e-prints* (2012), 1204.5413.
 - [29] A. N. Poddubny, P. A. Belov, and Y. S. Kivshar, *Phys. Rev. A* **84**, 023807 (2011).
 - [30] E. L. Ivchenko, Y. Fu, and M. Willander, *Phys. Solid State* **42**, 1756 (2000).
 - [31] I. H. Deutsch, R. J. C. Spreeuw, S. L. Rolston, and W. D. Phillips, *Phys. Rev. A* **52**, 1394 (1995).
 - [32] D. V. van Coevorden, R. Sprik, A. Tip, and A. Lagendijk, *Phys. Rev. Lett.* **77**, 2412 (1996).
 - [33] Y. Kagan, *Hyperfine Interactions* **123**, 83 (1999).
 - [34] E. M. Purcell and C. R. Pennypacker, *Astroph. J.* **186**,

- 705 (1973).
- [35] P. A. Belov and C. R. Simovski, *Phys. Rev. E* **72**, 026615 (2005).
- [36] M. G. Silveirinha and P. A. Belov, *Phys. Rev. B* **77**, 233104 (2008).
- [37] J. Korrying, *Physica* **13**, 392 (1947).
- [38] P. de Vries, D. V. van Coevorden, and A. Lagendijk, *Rev. Mod. Phys.* **70**, 447 (1998).
- [39] L. Landau and E. Lifshitz, *Electrodynamics of Continuous Media* (Pergamon, New York, 1974).
- [40] R. J. Pollard, A. Murphy, W. R. Hendren, P. R. Evans, R. Atkinson, G. A. Wurtz, A. V. Zayats, and V. A. Podolskiy, *Phys. Rev. Lett.* **102**, 127405 (2009).
- [41] P. A. Belov, R. Marqués, S. I. Maslovski, I. S. Nefedov, M. Silveirinha, C. R. Simovski, and S. A. Tretyakov, *Phys. Rev. B* **67**, 113103 (2003).
- [42] A. Savchenko and O. Savchenko, *Technical Phys.* **50**, 1366 (2005).
- [43] C. Kittel, *Introduction to Solid State Phys.* (Wiley, New York, 1996).
- [44] R. H. Swendsen and H. Callen, *Phys. Rev. B* **6**, 2860 (1972).
- [45] M. S. Tomaš and Z. Lenac, *Phys. Rev. A* **60**, 2431 (1999).
- [46] X.-H. Wang, Y. S. Kivshar, and B.-Y. Gu, *Phys. Rev. Lett.* **93**, 073901 (2004).
- [47] L. Novotny and B. Hecht, *Principles of Nano-Optics* (Cambridge University Press, New York, 2006).